Materials Advances

ROYAL SOCIETY OF CHEMISTRY

PAPER

View Article Online
View Journal | View Issue

Cite this: *Mater. Adv.*, 2025, 6, 9495

Microwave-assisted synthesis of graphene–ZnO (Gr–ZnO) nanorods for efficient solar photocatalytic removal of methylene blue as a model pollutant dye

Laura Khamkhash, † Alima Bazenova,† Kuralay Rustembekkyzy, Bachir Yaou Balarabe and Timur Sh. Atabaev *

Received 8th June 2025,
Accepted 12th October 2025

DOI: 10.1039/d5ma00612k

rsc.li/materials-advances

The widespread use of methylene blue (MB) dye in the textile industry contributes to environmental pollution, as it is hard to degrade and can pollute water and soil, negatively affecting aquatic life and ecosystems. This study presents the development of a graphene–ZnO nanorod-based (Gr–ZnO) photocatalyst through a combination of soaking and microwave-assisted synthesis suitable for efficient MB removal from water. It was found that the prepared Gr–ZnO photocatalyst consists of radially grown ZnO nanorods with a mean length of ~237 nm and a width of ~40 nm, growing from a common Gr sheet center. The synthesized Gr–ZnO photocatalyst exhibited remarkable photocatalytic performance, successfully degrading ~97.5% of an MB solution (V = 30 mL and C_o = 3 × 10^{-5} M) in just 40 minutes under solar irradiation by using only 3 mg of the photocatalyst. The effects of catalyst dosage, pH, and the presence of HCO_3^-, CO_3^{2-}, NO_3^-, and Cl^- anions were also evaluated to confirm the potential of the photocatalyst for real wastewater treatment. The potential mechanism of MB removal was examined and proposed with the help of radical scavengers. In conclusion, the synthesized Gr–ZnO photocatalyst was shown to be more effective as compared to other similar structures, underscoring its potential for wastewater treatment applications.

Introduction

Water pollution caused by organic dyes has emerged as a major global environmental concern. The release of dyes into water sources can damage aquatic ecosystems, threaten marine life, and create health hazards. Among them, methylene blue (MB) is commonly used as a dye in the textile industry, as well as in medicine as an antiseptic and for treating conditions like methemoglobinemia.[1,2] On the other hand, the MB dye in water can be toxic to aquatic life as it disrupts oxygen exchange and inhibits the respiratory processes of aquatic organisms, potentially leading to suffocation.[3] Moreover, it can accumulate in aquatic ecosystems, causing harm to the reproductive systems and growth of aquatic species, with long-lasting ecological effects.[4] Due to the difficulty of removing MB from wastewater using conventional techniques, researchers have investigated innovative and sustainable methods for its removal. One such method is the photocatalytic process using low-cost metal oxide catalysts, which has gained attention as a promising solution because it can harness sunlight energy to degrade harmful organic pollutants into CO_2 and H_2O.[5,6] Recently, zinc oxide (ZnO) has attracted considerable attention among other metal oxide catalysts because of its excellent photocatalytic efficiency, low-cost, non-toxic nature, and ability to regulate the morphology during the fabrication process.[7–9] However, ZnO also has some drawbacks, including limited sunlight absorption due to its high bandgap value (~3.3 eV) and a high rate of electron–hole recombination.[10,11] To address these challenges, coupling ZnO with 2D materials like graphene (Gr) or reduced graphene oxide (rGO) can be considered, as they can improve ZnO's photocatalytic activity by acting as electron acceptors and reducing electron–hole recombination rates.[12,13] Moreover, to enhance the specific surface area of the photocatalyst and capture more photons through light scattering effects, growing ZnO nanorods on the surface of 2D materials can be considered.

Although numerous studies on the preparation of 2D-ZnO composites can be found in the literature,[14,15] only a few have demonstrated the preparation and photocatalytic activity of 2D-ZnO nanorods. For example, Raub *et al.*[16] demonstrated that graphene oxide (GO) flakes coated onto the surface of ZnO nanorods can enhance the photocatalytic activity by

Department of Chemistry, School of Sciences and Humanities, Nazarbayev University, Astana 010000, Kazakhstan. E-mail: timur.atabaev@nu.edu.kz
† These authors contributed equally to this work.

approximately 5% under UVC exposure over a treatment period of 6 hours. The improved photocatalytic activity was attributed to better separation of charge carriers, as confirmed from photoluminescence (PL) analysis. ZnO nanorods deposited onto the surface of rGO sheets using an electrostatic method were found to exhibit higher photocatalytic activity compared to bare ZnO nanorods when tested against the rhodamine B (RhB) dye and phenol.[17] Xie *et al.*[18] demonstrated the fabrication of ZnO nanorods on the surface of rGO sheets through a hydrothermal method. It was found that the as-prepared rGO/ZnO nanorods exhibited superior removal of RhB and methyl orange (MO) dyes compared to bare ZnO nanorods. Despite the promising results so far, these composites are facing issues with gradual ZnO detachment from the surface of the 2D material. Moreover, the hydrothermal methods reported for the fabrication of rGO–ZnO nanorods[17,18] are time-consuming, highlighting the need for faster alternatives for fabricating 2D-ZnO nanorods.

Microwave-assisted synthesis has demonstrated itself as a fast, energy-efficient, and scalable method. In contrast to traditional synthesis methods, microwave irradiation offers uniform heating and speeds up reaction kinetics, enhancing the dispersion of composites and their structural integration.[19,20] For example, the rGO–ZnO/CuO nanocomposite,[21] prepared using a microwave-assisted method in a short period of time, proved effective for the catalytic reduction of 4-nitrophenol and the photocatalytic degradation of MB dye. Conversely, controlling the growth direction of ZnO nanorods remains a challenging task. Hence, our study focuses on presenting a relatively new method to control the directional growth of ZnO nanorods on 2D substrates, with graphene serving as a representative material. As a result, we successfully fabricated a Gr–ZnO photocatalyst composed of radially grown ZnO nanorods emerging from the common center of Gr sheets. This configuration not only facilitates better light trapping but also provides a higher number of accessible sites for improved photocatalytic activity. We believe that this methodology can be valuable for the construction of other 2D-ZnO nanorods, where 2D materials such as MXenes, MoS_2, and others can be used.

Methodology

Materials

Zinc acetate dihydrate ($Zn(CH_3COO)_2{\cdot}2H_2O$, 98.0%), graphene nanoplatelets (<2 μm), 2-propanol ($(CH_3)_2CHOH$, ≥99.5%), zinc nitrate hexahydrate ($Zn(NO_3)_2{\cdot}6H_2O$, 98%), hexamethylenetetramine ($(CH_2)_6N_4$, 99.9%), and methylene blue dye (MB, ≥95.0%) were purchased from Merck and used as received. High purity ethanol, nitrogen gas, Na_2CO_3, $NaNO_3$, NaCl, and $NaHCO_3$ were procured from local suppliers and used without any purification.

Characterization

The morphology of the Gr–ZnO nanorods was analyzed using SEM (Crossbeam 540, Carl Zeiss, Oberkochen, Germany) and TEM (JEM-1400 Plus, JEOL Ltd, Tokyo, Japan). Elemental analysis was performed with an EDS detector (Aztec analysis, Oxford Instruments, UK), while the Zn concentration was determined using ICP-OES (iCAP 6300 duo, Thermo Fisher Scientific Inc., Waltham, MA, USA). The crystal size, phase composition, and structural characteristics were examined using a SmartLab X-ray diffractometer (Rigaku, Tokyo, Japan) and a Raman spectrometer (LabRam HR evolution, Horiba, Kyoto, Japan). The surface area and pore size of the prepared photocatalyst were analyzed using an Autosorb iQ nitrogen porosimeter (Quantachrome Instruments, USA). Zeta potential values were measured using a Nanotrac Wave II/Zeta particle size analyzer (Microtrac Retsch GmbH, Germany). Absorbance of Gr and Gr–ZnO samples was recorded using an integrating sphere equipped on an absolute quantum yield spectrometer (C9920-02, Hamamatsu Photonics, Japan). Photoluminescence (PL) analysis was performed using a RF-6000 spectrofluorophotometer (Shimadzu Corporation, Japan).

Synthesis of Gr–ZnO nanorods

Gr powder (20 mg) was added to 4 mL of a zinc acetate solution in ethanol (5 mM), then dispersed through sonication and left in the dark for 1 h to allow the adsorption of zinc ions onto the surface of the Gr. Next, the Zn-adsorbed Gr was centrifuged at 8000 rpm for 5 min, gently washed with deionized (DI) water, and then dried in an oven at 80 °C for 24 h. The dried sample was then transferred to a conical glass flask fitted with a gas-tight stopper and two gas tubes. The atmospheric air was first replaced by purging N_2 gas into the flask for 30 min to prevent the oxidation of Gr to GO. Then, the flask was heated and maintained at 160 °C for 30 min to convert the Zn acetate into ZnO on the Gr surface. The process was repeated two times to ensure sufficient formation of the ZnO layer on the surface of Gr. The as-prepared Gr–ZnO composite was used as a source to grow the Gr–ZnO nanorods in the microwave synthesis step.

For the microwave synthesis, a precursor solution for the growth of ZnO nanorods was first prepared. Briefly, zinc nitrate (0.17 g) and hexamethylenetetramine (0.37 g) were dissolved in 50 mL of DI water, followed by 3 min of sonication. Afterward, 5 mL of precursor solution was mixed with 5 mg of Gr–ZnO powder and dispersed by sonication for 3 min. The mixture was then transferred to a 35 mL glass vessel and loaded into a CEM microwave synthesizer (CEM Corporation, USA). The reaction temperature was maintained at 90 °C for 20 minutes, while the microwave power was allowed to be controlled by the system. After the microwave treatment, the supernatant was removed, and the Gr–ZnO nanorods were gently washed several times with DI water before being dried at 70 °C in an oven.

Photocatalytic activity testing

The photocatalytic activity of the as-prepared Gr–ZnO nanorods was evaluated by degrading the MB dye under simulated solar light (LCS-100 simulator, 100 W, AM1.5G, Newport-Spectra Physics GmbH, Germany). The light intensity was adjusted to 1 sun using a commercial silicon reference cell. Varying amounts of Gr–ZnO nanorods were ultrasonically dispersed in

30 mL of an MB solution with a concentration of 3×10^{-5} M. The samples were then stirred magnetically for 1 h in the dark to ensure that adsorption–desorption equilibrium was reached between the photocatalyst and MB. The MB removal kinetics was determined at 664 nm using a UV-Vis spectrophotometer (Genesys 50, Thermo Fisher Scientific Inc., USA) as shown in Fig. S1 (SI). Each experiment was repeated three times to ensure the reproducibility of the results.

Results and discussion

Preparation and characterization of the photocatalyst

Fig. 1 illustrates the schematic diagram of the synthesis process. In step 1, zinc ions are incorporated onto the surface of Gr through the soaking method. In step 2, the incorporated Zn^{2+} ions are converted into ZnO on the surface of the Gr sheets during the thermal treatment process. To prevent oxidation of the Gr during the thermal treatment, the process was conducted under N_2 protection. In step 3, the precursor powder of Gr–ZnO is formed, setting the stage for the subsequent growth of Gr–ZnO nanorods. The formation of a ZnO seed layer on the surface of Gr is crucial for the subsequent growth of ZnO nanorods, as this seed layer provides nucleation centers and minimizes the lattice mismatch with the substrate.[22–24] Finally, in step 4, the growth of radially distributed ZnO nanorods occurs from the common seed layers on the surface of Gr.

To better understand the morphological characteristics of the Gr–ZnO nanorods, SEM and TEM imaging techniques were employed. SEM images (Fig. 2a and b) show that ZnO nanorods have been successfully synthesized, with the nanorods adhering uniformly to the graphene surface, facilitated by the presence of the ZnO seed layers. TEM analysis (Fig. 2c and d) was performed to further evaluate the morphological properties of the Gr–ZnO nanorods. TEM analysis results also confirm that the ZnO nanorods are uniformly distributed and well-formed. As shown in the inset of Fig. 2d, the nanorods are notably narrow, with average lengths of approximately 237 nm and widths of around 40 nm. In addition to directly influencing the surface area and aspect ratio, this configuration can also impact the catalytic activity and other functional properties of the Gr–ZnO nanorods.

The structural analysis of bare Gr and Gr–ZnO nanorods was conducted using XRD, and the obtained patterns are shown in Fig. 3a. The diffraction peak identified at 26.4° corresponds to the (002) plane of stacked graphene sheets (JCPDS no. 00-041-1487).[25] The diffraction peaks observed at 2θ = 31.7°, 34.4°, 36.3°, 47.5°, 56.6°, 62.8°, 66.4, 67.9°, 69°, and 76.9° correspond well to the (100), (002), (101), (102), (110), (103), (200), (112), (201), and (202) planes of zinc oxide, respectively. In particular, the obtained ZnO nanorods exhibited a wurtzite structure with the space group $P6_3mc$ (JCPDS no. 01-080-4433).[26] The mean crystallite size (D) was further determined using the well-known Scherrer equation. The mean crystallite size was determined to be approximately 13.40 nm for bare Gr and 36.75 nm for the Gr–ZnO nanorods. Dislocation density ($\delta = 1/D^2$), which reflects the number of defects in the sample,[7] was calculated to be 5.57×10^{-3} nm^{-2} for bare Gr and 1.32×10^{-3} nm^{-2} for Gr–ZnO nanorods, respectively. Next, the microstrain values (ε) for bare Gr and Gr–ZnO nanorods were evaluated using the Stokes–Wilson equation ($\varepsilon = \beta \cos\theta/4$), where β corresponds to the FWHM of the diffraction peak (radians) and θ represents the

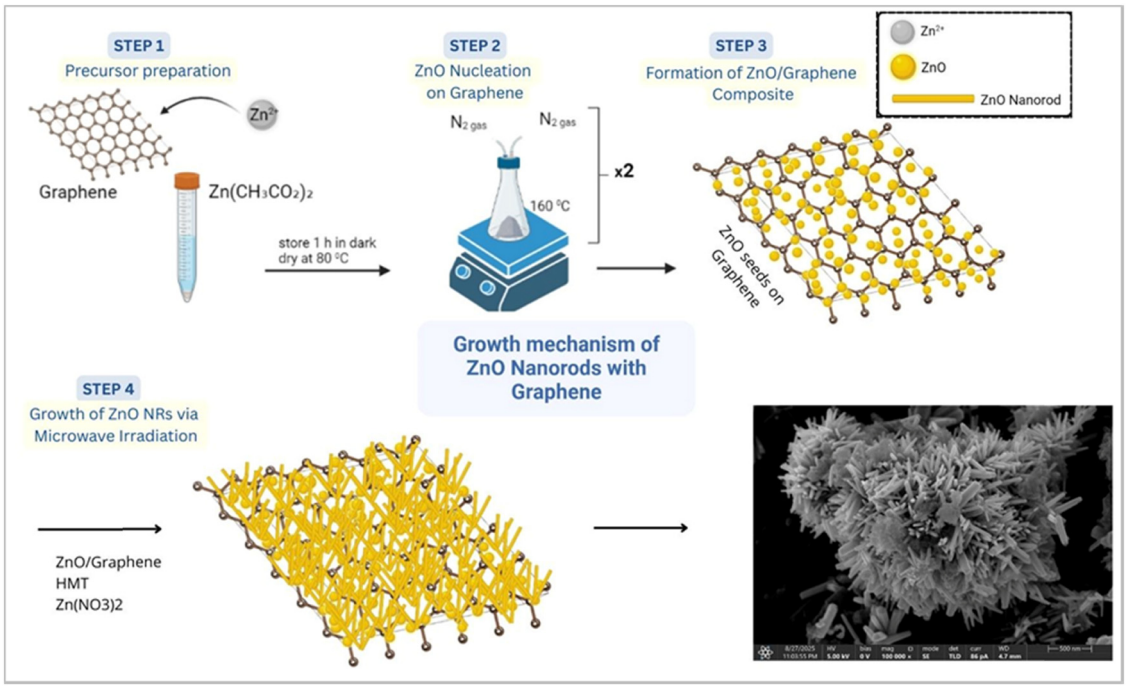

Fig. 1 Schematic diagram of the synthesis of Gr–ZnO nanorods.

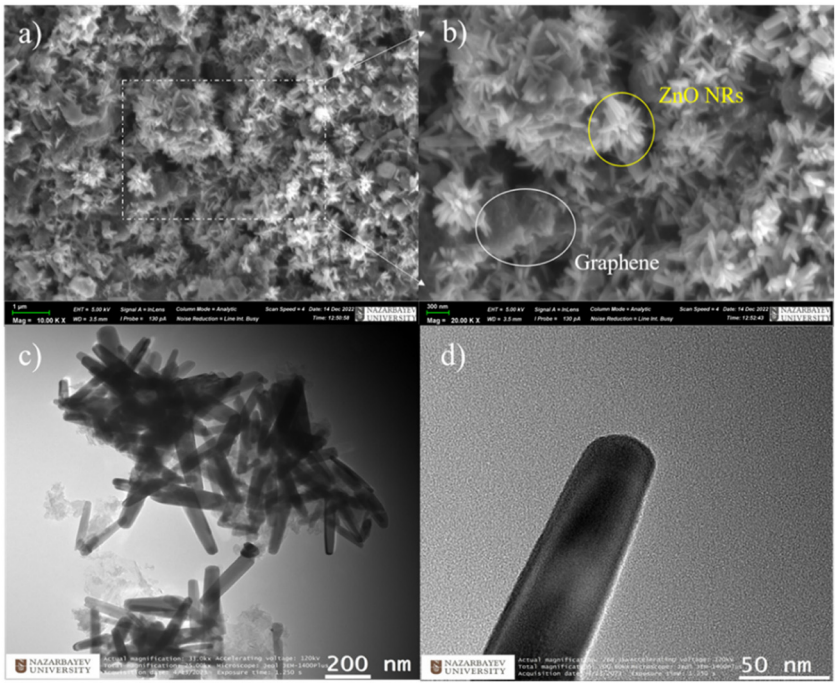

Fig. 2 (a) Low and (b) high-magnification SEM images and (c) low and (d) high-magnification TEM images of formed Gr–ZnO nanorods.

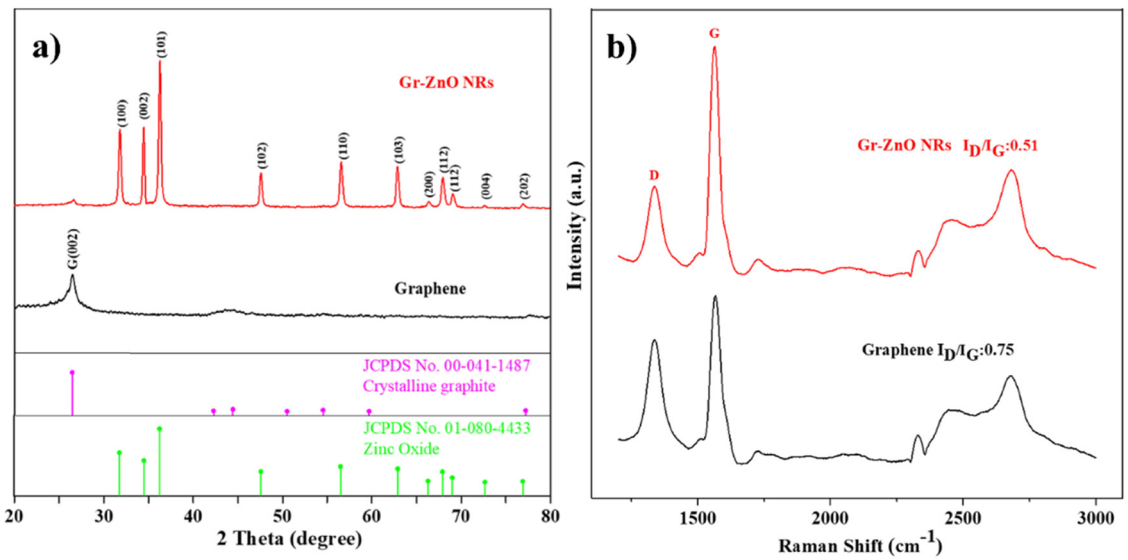

Fig. 3 (a) XRD patterns and (b) Raman spectra of bare Gr and Gr–ZnO nanorods.

Bragg diffraction angle.[7] The calculated microstrain values were 11.89 × 10^{-3} for bare Gr and 3.28 × 10^{-3} for the Gr–ZnO nanorods, respectively. Hence, the growth of ZnO nanorods on Gr significantly reduces dislocation density and microstrain, indicating improved crystallinity, enhanced lattice stability, and potentially superior functional performance compared to bare Gr. These conclusions were further verified by Raman spectroscopy. Fig. 3b reveals characteristic Raman signals for graphene-based materials at 1341 cm^{-1} and 1564 cm^{-1}, corresponding to the D and G bands, respectively. Typically, the D-band arises from structural imperfections caused by hydroxyl and epoxide groups on the carbon basal plane, while the G-band corresponds to the characteristic peak for sp^2 hybridized C–C bonds in graphene.[27,28] It can be observed that, upon the formation of Gr–ZnO nanorods, the intensity of the D band decreases in comparison to the G band. This change is also accompanied by a decrease in the I_D/I_G ratio, from 0.75 for bare Gr to 0.51 for the Gr–ZnO nanorods. We can speculate that the observed results may

be due to the thermal treatment under N_2 protection. Imperfections related to hydroxyl groups can be removed naturally under the influence of thermal treatment and N_2 flow and, while the number of epoxide groups can be reduced during the formation of ZnO seeds (oxygen groups can be combined with zinc ions). Hence, thermal treatment under N_2 protection is not only beneficial for ZnO seed formation on the Gr surface but also aids in fabricating Gr–ZnO nanorods with fewer defects in Gr. EDX elemental mapping (Fig. S2, SI) of the Gr–ZnO nanorods confirms a uniform distribution of C, Zn, and O elements throughout the analyzed region, suggesting consistent and uniform growth of ZnO nanorods on the graphene sheets.

Fig. 4a shows a characteristic Brunauer–Emmett–Teller type IV adsorption isotherm. The associated hysteresis loop highlights the mesoporous structure of the nanocomposite, as confirmed by the Barrett–Joyner–Halenda (BJH) analysis, which shows that the pore diameter ranges from ~3 to 47 nm (Fig. 4b, inset).[29] The pore volume was measured to be 0.22 $cm^3\ g^{-1}$, and the specific surface area of Gr–ZnO nanorods was found to be ~35.56 $m^2\ g^{-1}$.

Bare ZnO nanorods were also synthesized using a similar microwave methodology (without Gr) to serve as a reference sample. The optical properties of Gr–ZnO nanorods were assessed using absorbance and PL spectroscopy. Light absorbance (Fig. S3, SI) reveals that Gr–ZnO shows lower absorbance than Gr, which can be attributed to increased light scattering on the surface of ZnO nanorods. Tauc plot analysis determined the optical bandgap of Gr–ZnO to be 3.23 eV, which is close to the theoretical value of 3.3 eV for ZnO.[7,17] PL analysis (Fig. S4, SI) was carried out for Gr, Gr–ZnO, and bare ZnO nanorods for comparative purposes. The bare ZnO nanorods exhibit a broad emission peak starting at approximately 370 nm, which is attributed to the high electron–hole recombination rate, along with extended tails into the visible region that are typically associated with various intrinsic defects in ZnO. In contrast, Gr shows almost no emission in this region, while Gr–ZnO exhibits a weak emission similar to ZnO-related emission, though its intensity remains much closer to that of Gr. These observations suggest that effective charge separation occurs within the Gr–ZnO structure, which is considered to be advantageous for photocatalytic applications.

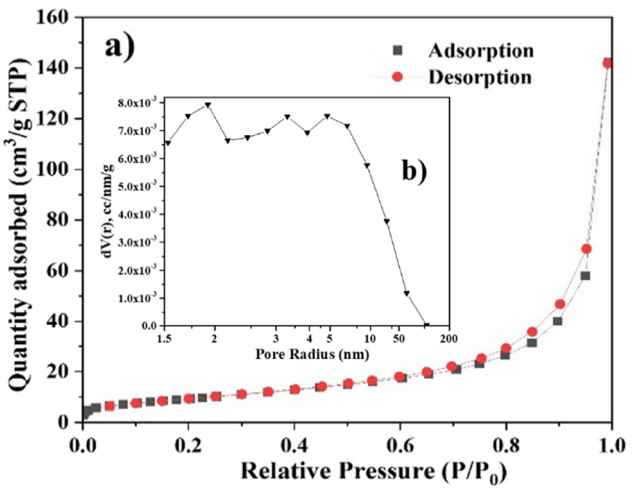

Fig. 4 (a) N_2 adsorption–desorption curves and (b) BJH curve measurement of Gr–ZnO nanorods.

Photocatalytic activity assessment of the photocatalyst

The photocatalytic activity of Gr–ZnO nanorods was monitored at room temperature in neutral pH under illumination from a solar simulator. Zeta potential measurements at neutral pH showed that the Gr–ZnO nanorods possess a negative surface charge of approximately −11.7 mV, which can facilitate the electrostatic attraction of cationic dyes such as MB. Other pH conditions were not investigated because of the amphoteric nature of ZnO, which makes it susceptible to etching in both acidic and basic media. First, a photocatalyst (3 mg) was dispersed in the MB solution and stirred in the dark for 60 minutes to achieve adsorption/desorption equilibrium. Next, the removal efficiency of the photocatalyst is evaluated using eqn (1):

$$\text{Removal efficiency (\%)} = (C_0 - C_t)/C_0 \times 100\% \quad (1)$$

where C_0 denotes the initial MB concentration, and C_t represents the residual MB concentration at different illumination intervals. Fig. 5a shows that the MB removal with Gr–ZnO nanorods reached approximately 97.5% after 40 minutes of solar light illumination, which was significantly higher compared to bare ZnO (~31.1%) and MB alone (~9.8%). This demonstrates that the incorporation of graphene notably enhances the MB removal rate. Moreover, the graphene provides more adsorption sites to MB molecules as it can be seen from the dark adsorption results. Specifically, the adsorption of MB on bare ZnO was found to be negligible (~1%), in contrast to the Gr–ZnO nanorods (~35%).

Eqn (2) was used to calculate the corresponding apparent reaction rates (k_a) for MB removal in the absence/presence of the photocatalysts *vs.* time (t).

$$\ln(C_0/C_t) = k_a t \quad (2)$$

The apparent reaction rates for bare MB, bare ZnO, and Gr–ZnO were found to be 0.0025, 0.0076, and 0.0858 min^{-1}, respectively (Fig. 5b). The linear plots indicated that the photocatalytic removal of MB followed a pseudo-first-order kinetic reaction. Table 1 presents a summary of previous studies on graphene, graphene oxide, or reduced graphene oxide–ZnO-based composites used for MB removal. Several key parameters, including catalyst dosage, MB concentration, reaction time, MB removal (%), light source, and reaction rates, were analyzed. Based on the literature review, the Gr–ZnO catalyst reported in this study appear to be one of the most efficient catalysts in terms of dosage used, time required for complete MB removal, light source, and reaction rate. For example, a significantly smaller amount of Gr–ZnO catalyst mass and time are required to degrade MB with a concentration of ~10 ppm, and the reaction can be performed directly under solar light exposure without using costly UV lamps. We attribute the enhanced performance of Gr–ZnO to several factors, including the intimate interfacial

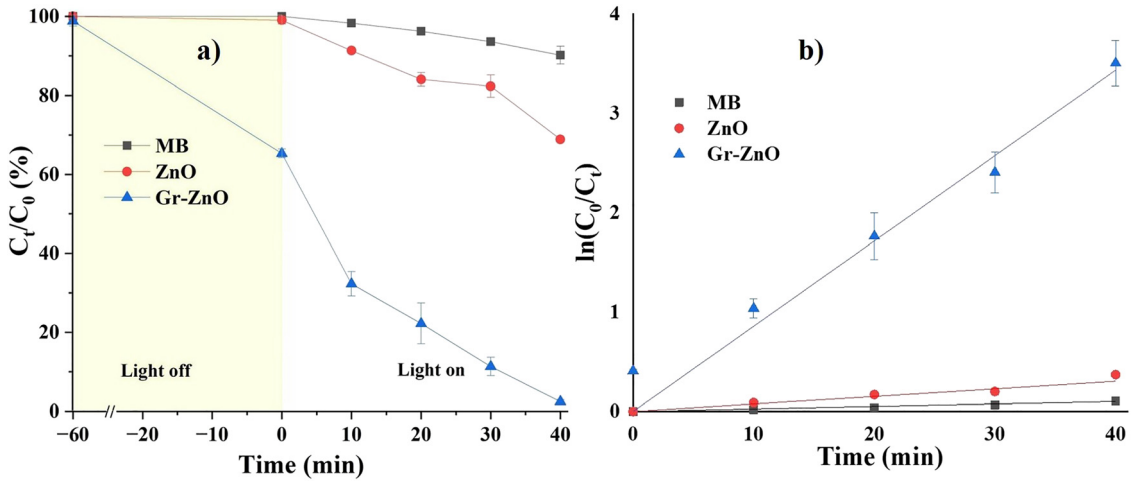

Fig. 5 (a) Photocatalytic removal and (b) apparent reaction rate determination for MB removal in the absence/presence of photocatalysts.

Table 1 Comparison of photocatalytic MB removal among different ZnO-based composites

Photocatalysts	Catalyst dosage (mg L^{-1})	MB (mg L^{-1})	Time (min)	MB removal (%)	Light source	k_a (min^{-1})	Ref.
Gr–ZnO	100	9.6	40	97.5	Solar simulator	0.086	This work
rGO@ZnO	200	15	100	99.0	Sunlight irradiation	0.040	30
ZnO/GO	1000	95, 95	80	91.0	Visible light	0.030	31
ZnO–rGO	2000	200	60	99.0	Visible light	0.090	32
rGO–Ag/ZnO	200	10	120	99.0	UV-Visible light	0.040	33
rGO–N–ZnO	1000	10	120	98.5	Visible light	0.030	34
ZnO–GO	500	20	90	97.6	UV light	0.030	35
Gr–ZnO	1000	10	60	87.0	Xenon lamp	0.034	36
ZnO–Gr	500	10	56	72.1	UV light	0.098	37
Gr/ZnO	500	10	180	74.3	Xenon lamp	0.005	38

contact between Gr flakes and ZnO nanorods, which significantly reduces microstrain in Gr and promotes more efficient charge separation, as supported by the XRD, Raman, and PL results. Moreover, a porous structure facilitates photon trapping, which enhances internal light scattering effects and consequently promotes the generation of additional charge carriers. Finally, the Gr–ZnO hybrid exhibits a unique 2D–1D architecture, in which the surface of each individual ZnO nanorod can effectively contribute to the photocatalytic activity.

The photocatalytic performance of ZnO-based catalysts is governed by various parameters, including the catalyst dosage, solution pH, and the presence of competing anionic species.[7–10] Fig. 6a illustrates the impact of different catalyst dosages on the removal efficiency of MB. It can be observed that the MB removal efficiencies at catalyst dosages of 3 mg and 5 mg (t = 40 min) were nearly identical, falling within the acceptable margin of an experimental error. On the other hand, a significant enhancement in MB removal efficiency was found when the catalyst dosage was increased to 10 mg, reaching approximately 99.86% within 10 min of reaction time. Such a substantial increase cannot be solely attributed to an accelerated photocatalytic reaction, as higher catalyst loading typically increases the turbidity of the suspension, which in turn promotes higher light scattering and consequently diminishes MB removal efficiency.[39] Hence, it can be inferred that the increased dosage of Gr–ZnO predominantly facilitated the adsorption of MB molecules onto the surface of the catalyst. To ensure the economical utilization of the catalyst, a dosage of 3 mg of Gr–ZnO nanorods was selected as the optimal concentration for all photocatalytic experiments.

Fig. 6b illustrates the influence of pH on the photocatalytic removal efficiency of MB. It is evident that the removal efficiency markedly decreases at pH 4, which can be attributed to the cationic nature of MB and the resulting competition between H^+ ions and MB molecules for adsorption sites.[40] Moreover, acidic conditions may promote the dissolution of ZnO nanorods, potentially leading to a substantial decline in photocatalytic removal activity. A recent study[41] reported that the point of zero charge (pH_{pzc}) of the GO–ZnO structure is approximately 6.98. At pH values above this threshold, the catalyst surface acquires a negative charge, thereby enhancing the electrostatic attraction between the catalyst and the cationic MB molecules. On the other hand, the removal efficiency of Gr–ZnO nanorods at pH 9 was observed to be lower than that at pH 7. This reduction in photocatalytic activity can be attributed to the amphoteric nature of ZnO, which renders it susceptible to partial dissolution under alkaline conditions, thereby compromising the structural integrity and active surface area

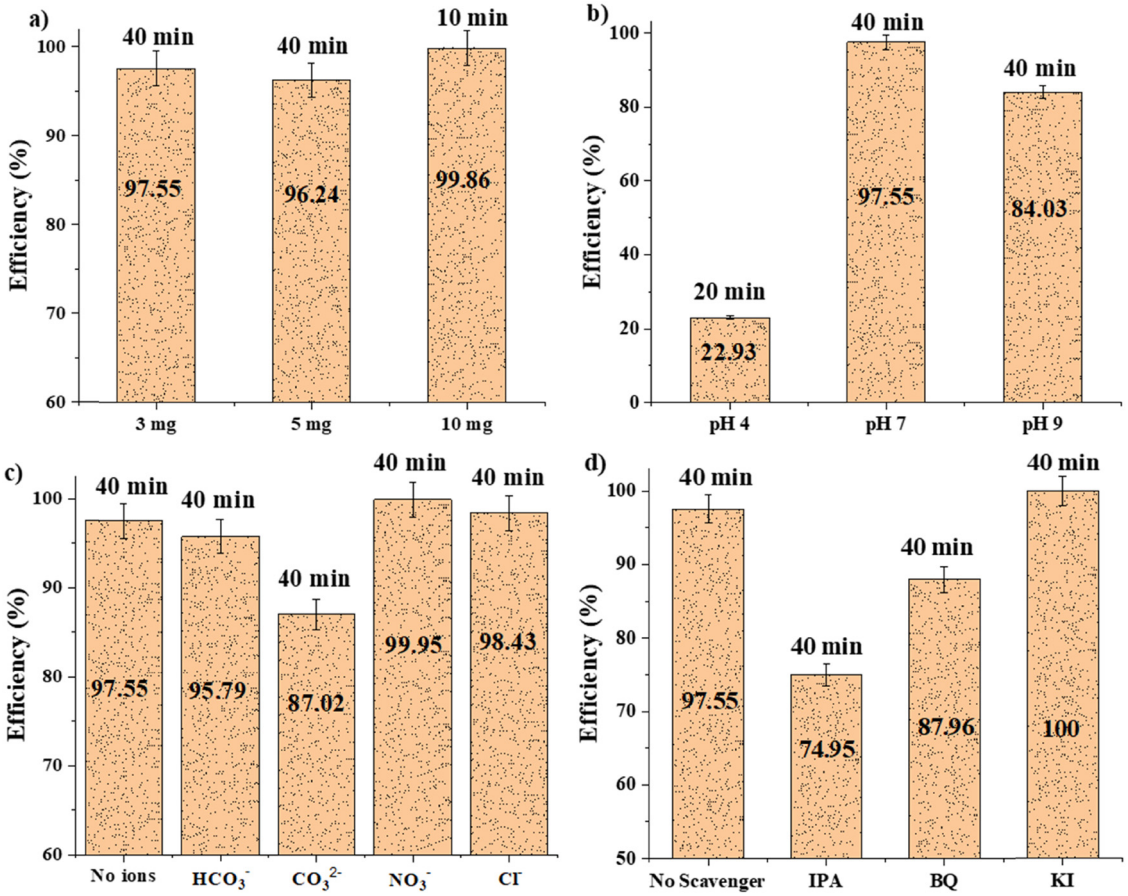

Fig. 6 Effects of (a) Gr–ZnO dosage, (b) solution pH, (c) the presence of various anions, and (d) various radical scavengers on MB removal efficiency.

of the catalyst. Therefore, the optimal pH for photocatalytic activity was determined to be ~7, a condition that can be readily attained through wastewater pH adjustment prior to treatment.

Given the presence of various ions in water, it is crucial to systematically assess the influence of the most prevalent anions on the photocatalytic performance of Gr–ZnO nanorods. In this study, several common anions, namely HCO_3^-, CO_3^{2-}, NO_3^-, and Cl^-, were investigated to evaluate their impact on the photocatalytic removal of MB. Fig. 6c shows that photocatalytic activity is slightly decreased in the presence of HCO_3^- and CO_3^{2-} anions. This observation can be attributed to the capture of $^\bullet OH$ radicals by bicarbonate and carbonate ions, leading to the formation of less reactive carbonate radicals.[42,43] Nevertheless, the overall photocatalytic performance of Gr–ZnO nanorods remains relatively high, indicating strong potential for the removal of cationic dyes from wastewater.

Fig. 6d shows the impact of several scavengers, including isopropanol (IPA), potassium iodide (KI), and benzoquinone (BQ), used to elucidate the predominant reactive species participating in the photocatalytic MB removal mechanism. According to the results, the addition of IPA, a well-established hydroxyl radical ($^\bullet OH$) scavenger, led to a pronounced decrease in MB removal efficiency, indicating that $^\bullet OH$ radicals play a pivotal role in the photocatalytic MB removal mechanism. Furthermore, BQ-induced quenching of $^\bullet O_2$ radicals also led to reduced removal efficiency, indicating their significant yet secondary role as compared to $^\bullet OH$ radicals. The addition of potassium iodide (KI), a hole (h^+) scavenger, resulted in minimal impact on MB removal efficiency, indicating that photogenerated holes play a minimal role in the photocatalytic process. Thus, the overall mechanism for MB removal can be represented by the following set of reactions:

$$\text{Gr–ZnO} + \text{light} \rightarrow e^- + h^+ \quad (3)$$

$$h^+ + H_2O \rightarrow {}^\bullet OH + H^+ \quad (4)$$

$$e^- + O_2 \rightarrow {}^\bullet O_2^- \quad (5)$$

$$2e^- + O_2 + 2H^+ \rightarrow H_2O_2 \quad (6)$$

$$e^- + H_2O_2 \rightarrow {}^\bullet OH + OH^- \quad (7)$$

$$h^+ + OH^- \rightarrow {}^\bullet OH \quad (8)$$

$$MB + {}^\bullet OH + {}^\bullet O_2^- \rightarrow H_2O + CO_2 \quad (9)$$

In the final step, the recyclability of the Gr–ZnO nanorods was evaluated over three consecutive cycles (Fig. S5, SI). It can be observed that the photocatalytic activity decreased significantly from ~97.5% to ~68.3% in the third cycle, which may be

attributed to photocorrosion and surface etching of the ZnO nanorods.[44] To support this claim, SEM analysis of the Gr–ZnO sample was performed after the third cycle, along with XRD and Raman characterization. The SEM image confirms that the ZnO nanorods underwent surface etching/photocorrosion on Gr sheets (Fig. S6, SI). However, XRD analysis (Fig. S7, SI) confirms that a certain amount of ZnO remains on the surface of the Gr sheets, which explains the continued photocatalytic activity, albeit at reduced efficiency. Additional Raman analysis (Fig. S8, SI) confirmed an increase in the I_D/I_G ratio from the initial 0.51 to 0.90, indicating oxidation of the Gr sheets, which is caused by the etching/photocorrosion of ZnO nanorods. Although the proposed Gr–ZnO nanorods do not exhibit very high recycling stability, their excellent photocatalytic efficiency and minimal catalyst requirement make them highly promising for potential wastewater treatment applications. Furthermore, the recycling stability could be enhanced by coating Gr–ZnO nanorods with a thin TiO_2 layer, which would protect the ZnO surface from etching/photocorrosion. This limitation can be addressed in a forthcoming study.

Conclusions

In this study, Gr–ZnO nanorods with outstanding photocatalytic performance under solar irradiation were successfully synthesized *via* a microwave-assisted method. The Gr–ZnO nanorods exhibited a mesoporous, flower-like morphology, with ZnO nanorods growing directly from the surface of graphene sheets. The photocatalytic performance of the synthesized structure was evaluated through MB removal, revealing that Gr–ZnO nanorods outperformed comparable 2D-ZnO materials with respect to catalyst dosage, reaction time, light source, and apparent removal rate. Additional experiments indicated that only a minimal amount of catalyst is required to achieve efficient performance under neutral pH (pH = 7) conditions, even in the presence of common anions such as HCO_3^-, CO_3^{2-}, NO_3^-, and Cl^-. The high photocatalytic efficiency can be attributed to the intimate interfacial contact between graphene sheets and ZnO nanorods, as well as the unique mesoporous, and flower-like morphology of the composite structure. Radical scavenging experiments revealed that both hydroxyl and superoxide radicals participate in the photocatalytic removal of MB, with hydroxyl radicals playing a dominant role. Thus, Gr–ZnO nanorods demonstrate considerable potential as effective photocatalysts for wastewater treatment and could provide valuable insights for the design of other advanced photocatalytic materials.

Conflicts of interest

The authors declare no conflicts of interest.

Data availability

The data supporting this article have been included as part of the supplementary information (SI). Supporting information: the graphical image of the setup employed for photocatalytic tests, EDX elemental mapping, total absorbance, Tauc plot, PL analysis, recyclability, SEM, XRD, and Raman analysis of recycled Gr–ZnO nanorods. See DOI: **https://doi.org/10.1039/d5ma00612k**.

Acknowledgements

This research was funded by the Science Committee of the Ministry of Science and Higher Education of the Republic of Kazakhstan (Grant No. AP19676347). This research was also funded by Nazarbayev University FDCRDG (Grant No. 20122022FD4111).

References

1 P. O. Oladoye, T. O. Ajiboye, E. O. Omotola and O. J. Oyewola, Methylene blue dye: Toxicity and potential elimination technology from wastewater, *Results Eng.*, 2022, **16**, 100678.
2 R. S. P. Mak and E. L. Liebelt, Methylene Blue: An Antidote for Methemoglobinemia and Beyond, *Pediatric Emergency Care*, 2021, **37**, 474–477.
3 A. K. Moorthy, B. G. Rathi, S. P. Shukla, K. Kumar and V. S. Bharti, Acute toxicity of textile dye Methylene blue on growth and metabolism of selected freshwater microalgae, *Environ. Toxicol. Pharmacol.*, 2020, **82**, 103552.
4 A. Tkaczyk, K. Mitrowska and A. Posyniak, Synthetic organic dyes as contaminants of the aquatic environment and their implications for ecosystems: A review, *Sci. Total Environ*, 2020, **717**, 137222.
5 A. Rafiq, M. Ikram, S. Ali, F. Niaz, M. Khan, Q. Khan and M. Maqbool, Photocatalytic degradation of dyes using semiconductor photocatalysts to clean industrial water pollution, *J. Ind. Eng. Chem.*, 2021, **97**, 111–128.
6 S. Khan, T. Noor, N. Iqbal and L. Yaqoob, Photocatalytic Dye Degradation from Textile Wastewater: A Review, *ACS Omega*, 2024, **9**, 21751–21767.
7 K. Rustembekkyzy, M. Sabyr, Y. N. Kanafin, L. Khamkhash and T. S. Atabaev, Microwave-assisted synthesis of ZnO structures for effective degradation of methylene blue dye under solar light illumination, *RSC Adv.*, 2024, **14**, 16293–16299.
8 S. Kumar, S. K. Sharma, R. D. Kaushik and L. P. Purohit, Chalcogen-doped zinc oxide nanoparticles for photocatalytic degradation of Rhodamine B under the irradiation of ultraviolet light, *Mater. Today Chem.*, 2021, **20**, 100464.
9 A. R. Bhapkar and S. Bhame, A review on ZnO and its modifications for photocatalytic degradation of prominent textile effluents: Synthesis, mechanisms, and future directions, *J. Environ Chem. Eng.*, 2024, **12**, 112553.
10 S. Em, M. Yedigenov, L. Khamkhash, S. Atabaev, A. Molkenova, S. G. Poulopoulos and T. S. Atabaev, Uncovering the role of surface-attached Ag nanoparticles in photodegradation

improvement of Rhodamine B by ZnO-Ag nanorods, *Nanomaterials*, 2022, **12**, 2882.
11 Y. S. Seo and S.-G. Oh, Controlling the recombination of electron-hole pairs by changing the shape of ZnO nanorods via sol-gel method using water and their enhanced photocatalytic properties, *Korean J. Chem. Eng.*, 2019, **36**, 2118–2124.
12 B. Y. Balarabe and T. S. Atabaev, Advancing photocatalysis: Insights from 2D materials and operational parameters for organic pollutants removal, *Adv. Sustainable Syst.*, 2024, **8**, 2400483.
13 A. Negash, S. Mohammed, H. D. Weldekirstos, A. D. Ambaye and M. Gashu, Enhanced photocatalytic degradation of methylene blue dye using eco-friendly synthesized rGO@ZnO nanocomposites, *Sci. Rep.*, 2023, **13**, 22234.
14 M. Darvishi, F. Jamali-Paghaleh, M. Jamali-Paghaleh and J. Seyed-Yazdi, Facile synthesis of ZnO/rGO hybrid by microwave irradiation method with improved photoactivity, *Surf. Interfaces*, 2017, **9**, 167–172.
15 N. Singhal, S. Selvaraj, Y. Sivalingam and G. Venugopal, Study of photocatalytic degradation efficiency of rGO/ZnO nano-photocatalyst and their performance analysis using scanning Kelvin probe, *J. Environ. Chem. Eng.*, 2022, **10**, 107293.
16 A. A. M. Raub, J. Yunas, M. A. Mohamed, B. Bais, A. A. Hamzah, J. Ridwan, J. Kazmi and M. A. Hassan, Synthesis and characterization of ZnO NRs with spray coated GO for enhanced photocatalytic activity, *Ceram. Int.*, 2022, **48**, 18238–18245.
17 F. Wang, Y. Zhou, X. Pan, B. Lu, J. Huang and Z. Ye, Enhanced photocatalytic properties of ZnO nanorods by electrostatic self-assembly with reduced graphene oxide, *Phys. Chem. Chem. Phys.*, 2018, **20**, 6959–6969.
18 M. Xie, D. Zhang, Y. Wang and Y. Zhao, Facile fabrication of ZnO nanorods modified with RGO for enhanced photodecomposition of dyes, *Colloids Surf., A*, 2020, **603**, 125247.
19 Y.-J. Zhu and F. Chen, Microwave-assisted preparation of inorganic nanostructures in liquid phase, *Chem. Rev.*, 2014, **114**, 6462–6555.
20 R. Krishnan, S. N. Shibu, D. Poelman, A. K. Badyal, A. K. Kunti, H. C. Swart and S. G. Menon, Recent advances in microwave synthesis for photoluminescence and photocatalysis, *Mater. Today Commun.*, 2022, **32**, 103890.
21 A. G. Bekru, L. T. Tufa, O. A. Zelekew, J. Gwak, J. Lee and F. K. Sabir, Microwave-Assisted synthesis of rGO-ZnO/CuO nanocomposites for photocatalytic degradation of organic pollutants, *Crystals*, 2023, **13**, 133.
22 T. S. Atabaev, Size-dependent water splitting activity of ZnO nanorods, *Mater. Today Proc.*, 2019, **6**, 15–18.
23 S. Fiedler, C. Ton-That and M. R. Phillips, Defect-free ZnO nanorods with high angular distribution for enhanced excitonic emission, *J. Mater. Res.*, 2023, **38**, 2145–2155.
24 F. Oke-Altuntas, S. Saritan and H. Colak, The effect of seed layer cycles on the structural, optical, and morphological properties of ZnO nanorods, *Microsc. Res. Tech.*, 2024, **87**, 2154–2170.
25 C. Hu, G. Zheng, F. Zhao, H. Shao, Z. Zhang, N. Chen, L. Jiang and L. Qu, A powerful approach to functional graphene hybrids for high performance energy-related applications, *Energy Environ. Sci.*, 2014, **7**, 3699–3708.
26 A. Bhuin, S. Udayakumar, J. Gopalarethinam, D. Mukherjee, K. Girigoswami, C. Ponraj and S. Sarkar, Photocatalytic degradation of antibiotics and antimicrobial and anticancer activities of two-dimensional ZnO nanosheets, *Sci. Rep.*, 2024, **14**, 10406.
27 L. Khamkhash, S. Em, A. Molkenova, Y.-H. Hwang and T. Atabaev, Crack-free and thickness-controllable deposition of TiO_2–rGO thin films for solar harnessing devices, *Coatings*, 2022, **12**, 218.
28 Z. Bo, X. Shuai, S. Mao, H. Yang, J. Qian, J. Chen, J. Yan and K. Cen, Green preparation of reduced graphene oxide for sensing and energy storage applications, *Sci. Rep.*, 2014, **4**, 4684.
29 L. López-Pérez, V. Zarubina and I. Melián-Cabrera, The Brunauer–Emmett–Teller model on alumino-silicate mesoporous materials. How far is it from the true surface area?, *Microporous Mesoporous Mater.*, 2021, **319**, 111065.
30 A. Negash, S. Mohammed, H. D. Weldekirstos, A. D. Ambaye and M. Gashu, Enhanced photocatalytic degradation of methylene blue dye using eco-friendly synthesized rGO@ZnO nanocomposites, *Sci. Rep.*, 2023, **13**, 22234.
31 S. A. Al-Zahrani, K. Umar, S. A. Tweib, J. A. M. Rashd, S. K. Afridi, S. A. Bhawani, A. A. Otaibi, N. Masood, D. Mansour, A. Khan and M. Ayyar, Biomass Mediated Synthesis of ZnO and ZnO/GO for the Decolorization of Methylene Blue under Visible Light Source, *Catalysts*, 2023, **13**, 409.
32 A. Nisar, M. Saeed, M. Muneer, M. Usman and I. Khan, Synthesis and characterization of ZnO decorated reduced graphene oxide (ZnO-rGO) and evaluation of its photocatalytic activity toward photodegradation of methylene blue, *Environ. Sci. Pollut. Res.*, 2021, **29**, 418–430.
33 N. Belachew, M. H. Kahsay, A. Tadesse and K. Basavaiah, Green synthesis of reduced graphene oxide grafted Ag/ZnO for photocatalytic abatement of methylene blue and antibacterial activities, *J. Environ. Chem. Eng.*, 2020, **8**, 104106.
34 M. Suresh and A. Sivasamy, Fabrication of graphene nanosheets decorated by nitrogen-doped ZnO nanoparticles with enhanced visible photocatalytic activity for the degradation of Methylene Blue dye, *J. Mol. Liq.*, 2020, **317**, 114112.
35 Y. Lin, R. Hong, H. Chen, D. Zhang and J. Xu, Green synthesis of ZnO-GO composites for the photocatalytic degradation of methylene blue, *J. Nanomater.*, 2020, **2020**, 147357.
36 R. A. Mahmud, A. N. Shafawi, K. A. Ali, L. K. Putri, N. I. M. Rosli and A. R. Mohamed, Graphene nanoplatelets with low defect density as a synergetic adsorbent and electron sink for ZnO in the photocatalytic degradation of Methylene Blue under UV–vis irradiation, *Mater. Res. Bull.*, 2020, **128**, 110876.
37 H. Fan, X. Zhao, J. Yang, X. Shan, L. Yang, Y. Zhang, X. Li and M. Gao, ZnO–graphene composite for photocatalytic degradation of methylene blue dye, *Catal. Commun.*, 2012, **29**, 29–34.
38 J. Zhang, Y. Yang, X. Huang, Q. Shan and W. Wu, Novel preparation of high-yield graphene and graphene/ZnO composite, *J. Alloys Compd.*, 2021, **875**, 160024.

39 I. Groeneveld, M. Kanelli, F. Ariese and M. R. Van Bommel, Parameters that affect the photodegradation of dyes and pigments in solution and on substrate – An overview, *Dyes Pigm.*, 2022, **210**, 110999.
40 S. Yamaguchi, S. Minbuta and K. Matsui, Adsorption of the cationic dye methylene blue on anodic porous alumina in sodium dodecyl sulfate solutions, *Langmuir*, 2020, **36**, 4592–4599.
41 S. Singh, A. G. Anil, S. Khasnabis, V. Kumar, B. Nath, V. Adiga, T. S. S. K. Naik, S. Subramanian, V. Kumar, J. Singh and P. C. Ramamurthy, Sustainable removal of Cr(VI) using graphene oxide-zinc oxide nanohybrid: Adsorption kinetics, isotherms and thermodynamics, *Environ. Res.*, 2021, **203**, 111891.
42 C. L. Bianchi, B. Sacchi, C. Pirola, F. Demartin, G. Cerrato, S. Morandi and V. Capucci, Aspirin and paracetamol removal using a commercial micro-sized TiO_2 catalyst in deionized and tap water, *Environ. Sci. Pollut. Res.*, 2016, **24**, 12646–12654.
43 S. Yan, Y. Liu, L. Lian, R. Li, J. Ma, H. Zhou and W. Song, Photochemical formation of carbonate radical and its reaction with dissolved organic matters, *Water Res.*, 2019, **161**, 288–296.
44 M. Dimitropoulos, C. A. Aggelopoulos, L. Sygellou, S. T. Tsantis, P. G. Koutsoukos and S. N. Yannopoulos, Unveiling the photocorrosion mechanism of zinc oxide photocatalyst: Interplay between surface corrosion and regeneration, *J. Environ. Chem. Eng.*, 2024, **12**, 112102.